JACS
JOURNAL OF THE AMERICAN CHEMICAL SOCIETY

Perspective

pubs.acs.org/JACS

Graphene and Graphene-like Molecules: Prospects in Solar Cells

Kian Ping Loh,* Shi Wun Tong, and Jishan Wu

Department of Chemistry and Centre for Advanced 2D Materials, National University of Singapore, 3 Science Drive 3, 117543 Singapore

ABSTRACT: Graphene is constantly hyped as a game-changer for flexible transparent displays. However, to date, no solar cell fabricated on graphene electrodes has out-performed indium tin oxide in power conversion efficiency (PCE). This Perspective covers the enabling roles that graphene can play in solar cells because of its unique properties. Compared to transparent and conducting metal oxides, graphene may not have competitive advantages in terms of its electrical conductivity. The unique strength of graphene lies in its ability to perform various enabling roles in solar cell architectures, leading to overall improvement in PCE. Graphene can serve as an ultrathin and transparent diffusion barrier in solar cell contacts, as an intermediate layer in tandem solar cells, as an electron acceptor, etc. Inspired by the properties of graphene, chemists are also designing graphene-like molecules in which the topology of π-electron array, donor−acceptor structures, and conformation can be tuned to offer a new class of light-harvesting materials.

INTRODUCTION

Graphene, an atomic layer of carbon arranged in a honeycomb lattice, has inspired a whole new generation of research on the physics of two-dimensional materials. Right from the early days, photovoltaics had already been considered as a promising area for the use of graphene. Could graphene be considered a next-generation electrode for organic photovoltaic devices (OPVs)? The optical transparency, high carrier mobility, flexibility, and large-scale processibility of graphene have frequently been cited as reasons for applying it as transparent and conducting electrodes in solar cells.[1−6] Table 1 compares the performance of graphene to that of carbon nanotubes (CNTs) and silver-based transparent and conducting electrodes, and it can be seen that graphene is indeed very competitive. However, no OPV containing a graphene electrode has out-performed indium tin oxide (ITO) to date, although recent results show that the performance gap is closing.[7] For real-world applications to come to fruition, we have to exploit the strengths of graphene. It is our perspective that graphene can be used not just as electrodes but as different components in the solar cell, to serve a diverse range of functions (Figure 1). This calls for different processing methods for graphene. On the other hand, a new class of graphene-like molecules have been synthesized that offer reasonably high performance compared to traditional, full-erene-based bulk heterojunctions. There is plenty of rooms for further developments in terms of the synthetic versatility and structural diversity of these graphene-like molecules.

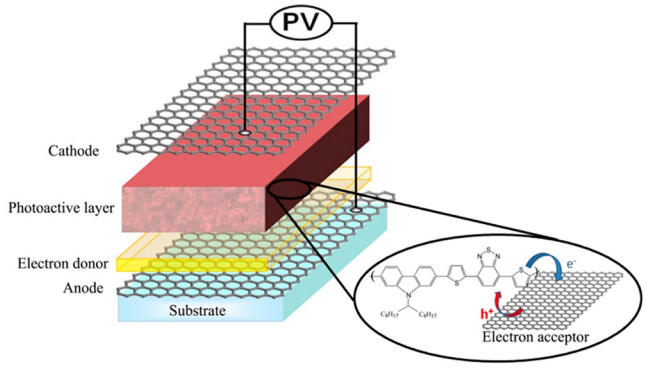

Figure 1. Graphene that has been treated appropriately can be used as different components in a solar cell, including cathode, anode, and photoactive layers.

GRAPHENE AS A TRANSPARENT ELECTRODE

Coating graphene on a glass or polymer support to fabricate a transparent conducting electrode allows conventional OPV configurations to be tested (Table 1).[8−11] However, a fundamental material limitation hinders this possibility. The sheet resistance of graphene can be derived as $R_s = (\sigma_{2d}N)^{-1}$, where N is the number of layers and σ_{2d} is the conductivity of the 2-D sheet. It is calculated as ∼6.4 kΩ for monolayer graphene, which is far inferior to that of ITO.[12] In theory, stacking graphene in a layer-by-layer manner can improve the sheet conductivity. However, multi-layer graphene is constrained by the trade-off between conductivity and transparency. The thickness of the graphene used typically cannot exceed four layers, since three-layer graphene has an experimentally measured sheet resistance of ∼300 Ω/sq and a transparency of ∼92% at λ = 550 nm.[7] These values are respectable but lag behind those of many sputtered metal oxide films.

Despite this limitation, there are attractive arguments for the use of graphene as an electrode. Being an atomic sheet consisting of only surfaces, graphene's Fermi level, carrier density, and work function can be readily tuned by surface treatment; thus, it can be used as either an anode or a cathode. The ambipolar nature of graphene does not allow it to show good rectification characteristics unless an appropriate surface treatment is carried out to block electron or hole injection. Doping may also be necessary, both to increase the carrier concentration and to shift the Fermi level of graphene for efficient carrier extraction across the interface with the active layer.[1]

Received: October 19, 2015
Published: December 10, 2015

DOI: 10.1021/jacs.5b10917
J. Am. Chem. Soc. 2016, 138, 1095−1102

Table 1. Photovoltaic Performance of Solar Cell Devices with Graphene, Silver Nanowire, or Carbon Nanotube Electrodes[a]

material	synthesis process	role	PCE (%)	device	ref
CVD SLG	chemical vapor deposition	cathode	7.1	OPV	8
SLGNRs (Au-doped)	SLGNRs from EBL patterned on CVD SLG and further doped with $AuCl_3$	anode	8.48	OPV	9
rGO	GO from modified Hummer's method reduced at 150 °C	anode	8.02	OPV	10
rGO (Cl-doped)	GO from modified Hummer's method reduced and doped by UV irradiation in the presence of a Cl_2 gas	anode	6.56	OPV	11
CVD SLG ($AuCl_3$-doped)	chemical vapor deposition	anode	15.6	G/n-Si	24
CVD SLG	chemical vapor deposition	cathode	10.5	G/p-Si	25
VACNTs/MLG	VACNTs grown on MLG by chemical vapor deposition	cathode	8.2	DSSCs	26
CNTs	chemical vapor deposition	cathode	5.81	DSSCs	27
CNTs (HNO_3-doped)	lamination	anode	6.32	perovskite	28
CNTs (MoO_x-doped)	lamination	anode	6.04	OPV	29
CNTs (HNO_3-doped)	drop-casting	anode	4.4	OPV	30
GO:AgNWs/PEDOT:PSS	GO from modified Hummer's method; AgNWs:GO solution spin-coated onto PEDOT:PSS	anode	13.3	PEDOT/n-Si	32
SLG-AgNWs:GO	SLG transferred onto spin-coated AgNWs:GO	anode	8.68	G/n-Si	33
AgNWs	spin-coating	anode	5.8	OPV	34
CP-AgNW/cPI	layer-by-layer spin-coating	anode	7.42	OPV	35

[a]Abbreviations: CVD SLG, chemical vapor deposited single-layer graphene; SLGNRs, single-layer graphene nanoribbons; EBL, electron beam lithography; ARC, anti-reflective coating; VACNTs, vertically aligned carbon nanotubes; MLG, multi-layer graphene; AgNWs, silver nanowires; PEDOT:PSS, poly(3,4-ethylenedioxythiophene)-poly(styrenesulfonate); and CP-AgNW/cPI, a conductive polymer−silver nanowire composite embedded in a colorless polyimide matrix.

Why not use thicker graphene sheets to achieve higher conductivity? At present, it is not easy to control the uniformity of multi-layer graphene grown by chemical vapor deposition (CVD). For layer-by-layer stacked CVD graphene, the expected scaling behavior between thickness and conductivity is often compromised by the poor electronic coupling between the stacked CVD graphene sheets owing to the presence of organic residues and trapped air pockets from the transfer process. These problems are amplified in large-area electronic devices, where the series resistance scales with the lateral dimension. Unless special care is taken, transferred graphene films are rarely wrinkle-free. Wrinkles are produced by capillary forces during wet transfer; they trap air pockets and prevent good electronic coupling between the graphene layers. There is a need to "iron out" wrinkles in graphene and "hot press" the graphene sheets to ensure that the distance between the layers is within the typical van der Waals bonding distance. Recently, we have shown that the plane-to-plane tunneling conductivity of stacked CVD graphene layers can be improved by several orders of magnitude by inserting a self-assembled monolayer (1-pyrenebutyric acid *N*-hydroxysuccinimide ester) between the graphene layers.[13] The molecular layer plays dual roles as a molecular bridge between the stacked layers and a hole-dopant for the graphene. The strong binding between the molecules and the graphene also supplants polymeric transfer residues on the graphene surface, leading to greater planarization of the graphene.

Major efforts have been directed at improving the sheet conductivity of graphene by doping. Most of these qualify as "quick and dirty" chemical methods in which nitric acid, tetracyanoquinodimethane, and $AuCl_3$ are commonly used.[14−16] However, exposure to air and moisture results in degradation of the doping effect with time. Clearly, a more robust way of doping is needed for realizing long-term stability. Ozyilmaz and Ahn[17] achieved this by supporting an OPV on an ultrathin ferroelectric film. The non-volatile electrostatic potential created by dipoles in the ferroelectric polymer poly(vinylidene fluoride-*co*-trifluoroethylene) dopes the graphene (70 Ω/sq at 87% transparency). Supporting graphene on polymer substrates offers the added advantages of flexibility, good mechanical stability, and durability.

Thermal annealing in a controlled oxygen atmosphere induces ~10^{13} cm^{-2} p-type doping of graphene. However, further reactivity in ambient atmosphere sometimes creates instability due to permeation of adsorbates between graphene and the substrate. The influence of ambient adsorbates on defects in graphene leads to an overall offset toward p-doping, masking intrinsically n-doped samples. Owing to this, the stable n-type doping of graphene is more challenging than p-doping, and the performance of devices with n-doped graphene junctions is typically low.[18] The photoinduced doping of graphene under light illumination provides another strategy to achieve stable, on-demand doping. For example, the photoinduced modulation of doping in graphene/boron nitride heterostructures, where the dopants were separated from the conducting channel, resulted in a controllable n-type transport behavior of graphene with the preservation of high mobility under visible light illumination.[19]

To date, when organic photoactive dyes have been used, graphene-on-glass electrodes have not outperformed the power conversion efficiency (PCE) of ITO. In addition to the need for good conductivity and transparency, the interface energy offset between graphene and the photoactive material has to be matched to optimize charge transfer. Surface wettability is another problem as the hydrophobic graphene prevents certain hole or electron transport layers from being coated well. Time-resolved surface photoresponse measurements show that p-doped graphene actually extracts electrons and competes with acceptor molecules for electron extraction; thus, it functions better as a cathode.[20] Recently, Gradečak et al. showed that coating graphene with an appropriately treated electron-blocking or transport layer is critical for its use as an anode or a cathode.[7] On a conventional anode-based OPV architecture using poly(3,4-ethylenedioxythiophene)-poly(styrenesulfonate) (PEDOT:PSS) as a hole injection layer and PTB7/$PC_{71}BM$ as the photoactive layer, they showed that thermally annealing the electron-blocking MoO_3 layer before spin-coating the organic photoactive layer allows a record-high PCE (6.1%) to be attained for a graphene anode, which is closely comparable with that of an

DOI: 10.1021/jacs.5b10917
J. Am. Chem. Soc. 2016, 138, 1095−1102

ITO reference electrode (PCE = 6.7%). They also demonstrated the use of graphene in an inverted cathode-based solar cell using n-type ZnO as the electron transport layer, where the device performance also approached that of ITO.

GRAPHENE SCHOTTKY BARRIER CELLS

Moving beyond the use of graphene-on-glass or graphene-on-polymer, the innovative use of graphene in other types of solar cell architectures has begun to emerge. Such efforts take advantage of graphene's tunable work function and its diffusion-barrier properties. Several niche applications have been demonstrated for graphene in various solar cell architectures, ranging from silicon p-n solar cells to their Schottky barrier counterparts.

In a conventional silicon p-n junction solar cell, the diffusion of metals from the metal contacts into Si can cause unwanted doping and lead to the formation of deep trap levels. Cu and Au, which are among the most widely used interconnects, diffuse significantly into Si. The use of a dielectric barrier such as TaN or TiN is undesirable, as it can change the junction properties. Commercial Si-based solar cells avoid this problem by substituting Cu with expensive Ag, as the latter diffuses more slowly. Graphene is found to be an excellent protective barrier against Cu and Al diffusion, and it does not modify the Schottky barrier of copper on silicon.[21] In addition, graphene is atomically thin and allows electrons to tunnel through it easily. Thus, graphene can be employed as a diffusion barrier for copper electrodes and as interconnects in solar cells.

Extending beyond this, graphene can also be used effectively as a top electrode in Schottky barrier solar cells. In a traditional Schottky barrier cell, a thin transparent metal layer is deposited on an n-type silicon interface, leading to a positively charged depletion region as donor electrons are transferred across the interface. In a graphene Schottky barrier solar cell, graphene replaces the metal, and the barrier height is given essentially by the difference in work function between graphene and the n-doped semiconductor.[22,23] One advantage is that graphene's Fermi level and work function can be readily tuned by doping. Song et al. reported a new record efficiency of 15.6% in CVD graphene anode/n-silicon devices with an anti-reflective coating and suitably doped graphene.[24] By doping the graphene with $AuCl_3$ and carefully optimizing the silicon oxide thickness at the graphene/Si interface to minimize carrier recombination, a higher fill factor can be attained. To achieve stable doping, the concept of sunlight-activated, tunable n-doping of graphene was demonstrated by Chen et al., who developed a graphene/TiO_x cathode to be used in a graphene/Si Schottky junction solar cell.[25] With its intrinsic n-type doping, the TiO_x thin layer acts as an electron-donating agent, increasing the electron concentration and the Fermi level of graphene. Upon illumination, photoexcited electrons from TiO_x are transferred to graphene, further increasing the n-doping and Schottky barrier heights at the graphene/p-Si junction. A good PCE (>10%) can be obtained. It can be appreciated that such photoinduced doping of graphene under light illumination provides a more stable form of doping than chemical doping.[25]

Another emerging area is the use of graphene as a cathode in dye-sensitized solar cells (DSSCs). Dong et al. reported a novel cathode made from 150-μm-long CNTs grown on catalyst-covered graphene, which has the potential to replace the expensive and brittle platinum-based materials used in conventional DSSC photovolatics.[26] Numerous reports have shown that stand-alone CNTs can act as good electrodes in solar cells, with efficiency ranging from 4.4% to 6.32% (Table 1).[27−30] A hybrid graphene/CNT electrode has lower charge-transfer resistance with the electrolyte (20 times smaller than for platinum-based cathodes) owing to its large surface area. DSSCs utilizing this flexible, vertically aligned CNT/graphene hybrid cathode outperformed Pt-based cells in both rigid (8.2% vs 6.4%) and flexible (3.9% vs 3.4%) assemblies.

The above discussion is based on graphene grown by CVD with the hope that roll-to-roll growth-and-transfer technology will address the scaling issues faced in the implementation of large-area devices. Parallel to CVD graphene, numerous research efforts have focused on liquid-phase exfoliated graphene or graphene oxide (GO). Owing to its defective and insulating nature, the sheet resistance of GO or reduced graphene oxide (rGO) is too high to compete against ITO; however, its solution-processibility opens up many alternative functions, such as hole transport and charge relay. GO is particularly well suited as a matrix for supporting conducting silver nanowires (AgNWs). For example, insulating GO flakes have been used as an overcoating layer and protecting layer for a conductive-nanowire-based indium-free transparent conductive film, in which large-area scalability has been demonstrated.[31] The sandwich structure formed by a AgNWs network between PEDOT:PSS and GO was reported to have lower resistivity than ITO,[32] and a high PCE = 13.3% could be obtained, which is better than that of electrodes fabricated entirely from AgNW composites (Table 1).[33−35] Chhowalla et al. also demonstrated that GO, which can be deposited from a neutral solution and is non-damaging to ITO, is as efficient as PEDOT:PSS in terms of functioning as a hole transport and electron blocking layer in an OPV device.[36]

GRAPHENE IN PEROVSKITES-BASED SOLAR CELL

Recently, a new type of solar cell based on organic−inorganic halide perovskites has witnessed rapid development. Although further optimization seems possible, its PCE has already surpassed 20% since its first development in 2009. Graphene can be utilized to improve the device performance and yield during the fabrication of perovskite-based solar cells.[37−40] For example, the use of high-temperature sintered TiO_2 as the electron transport layer in perovskite-based solar cells is disadvantageous, owing to its high cost and slow production. To address this, Wang et al. employed low-temperature processed nanocomposites of pristine graphene nanoflakes and anatase-TiO_2 nanoparticles in the electron transport layer in perovskite-based solar cells.[37] Remarkable photovoltaic performance with efficiency up to 15.6% is achievable with this nanocomposite, owing to the good energy level alignment between graphene and its adjacent layers (fluorine tin oxide and TiO_2) as well as the good carrier mobility of graphene. Graphene can also be used to extract electrons efficiently from TiO_2, thus leaving fewer electrons in TiO_2 to undergo recombination with the holes in perovskites. Printable inks made from conducting graphene and TiO_2 nanoparticles should be highly useful in printable solar cell technology. The integration of metal trihalide perovskites[37] and graphene may lead to the development of a printable, roll-to-roll process for the large-scale manufacturing of a new type of solar cell, where graphene plays the dual roles of passivating layer and electrode to the perovskite.

DOI: 10.1021/jacs.5b10917
J. Am. Chem. Soc. 2016, 138, 1095−1102

Table 2. Photovoltaic Performance for the Devices with Graphene, Silver Nanowire, or Carbon Nanotubes Intermediate Layers in Tandem Organic Photovoltaic Solar Cells[a]

intermediate layer	synthesis process	PCE (%)	ref
PEDOT:PSS/Au/V_2O_5	PEDOT:PSS, spin-coating	4.8 (series)	42
	Au/V_2O_5, thermal evaporation		
MoO_3/Al/Ag/MoO_3	thermal evaporation	3.1 (parallel)	43
LiF/Al/Au	thermal evaporation	2.4 (series)	44
		2.5 (parallel)	
CVD MLG/MoO_3	MLG, chemical vapor deposition	2.3 (series)	48
MoO_3/CVD MLG/MoO_3	MoO_3, thermal evaporation	2.9 (parallel)	
GO:PEDOT:PSS/ZnO	spin-coating	4.14 (series)	49
ZnO/GO:CNTs	spin-coating	4.10 (series)	50
GO-Cs/Al/GO/MoO_3	GO-Cs and GO, spin-coating	3.91 (series)	51
	Al and MoO_3, thermal evaporation		
ZnO/PEDOT:PSS/AgNW/ZnO	doctor-blading	4.25 (parallel)	45
PEDOT:PSS/CNTs/PEDOT:PSS	PEDOT:PSS, spin-coating	0.31 (parallel)	46
	CNTs dry-drawn laterally from CVD-grown oriented CNTs forest		
CNTs	Transferred from CVD-grown CNTs sheet	1 (series)	47
		2.33 (parallel)	

[a]Abbreviations: PEDOT:PSS, poly(3,4-ethylenedioxythiophene)-poly(styrenesulfonate); V_2O_5, vanadium(V) oxide; MLG, multi-layer graphene; GO-Cs, cesium-neutralized graphene oxide.

GRAPHENE AS INTERMEDIATE LAYERS IN TANDEM CELLS

The tandem solar cell concept boosts device efficiency by stacking two or more single-junction cells with different band gaps, such that the effective absorption window is the combination of them all. An intermediate layer (IML) is needed to join the stacked cells so that they can harvest complementary absorption spectra without significant optical and electronic losses. Generally, an efficient IML must fulfill three requirements: (i) act as a good recombination layer for electron and holes, (ii) have minimal light absorption, and (iii) act as a protective layer to prevent intermixing of two subcells. To prevent intermixing problems, the IML has to be a continuous, compact layer. Hadipour et al. reported that the thinnest continuous metal layer required to protect the bottom device from being destroyed during the fabrication of the top device is 10−15 nm.[41] Although such thick metal layers can act as a protective and conductive IML in the parallel tandem cells, the 40−60% loss in light transmission due to the poor transparency of Au,[42] Al/Ag,[43] and Al/Au[44] becomes a disadvantage.

Transparent IMLs consisting of AgNW films[45] or CNTs films[46,47] have been developed to replace the conventional metal IML (Table 2). They can be solution-processed and afford a light transmission of >80%, which is better than that possible with metal contacts. However, the high surface roughness of AgNWs and the large contact resistance between CNTs/organic materials pose problems for their use as IMLs. Due to its transparency, high conductivity, multi-layer CVD graphene has been utilized as IML in both series-connected and parallel-connected tandem OPV devices (Figure 2a).[48] Thus far, most IMLs employ a series connection rather than a parallel connection, owing to the limited availability of IMLs with high in-plane conductivity. In a series-connected tandem cell, a discontinuous metallic IML is sufficient to ensure efficient recombination between two subcells. In contrast, the IML is required to act as a highly conductive, transparent, and continuous electrical contact in parallel connection because of the lateral flow of current. Indeed, there is a strong demand to develop parallel-connected tandem cells in which two subcells can operate individually. Compared with series-connected tandem cells, high efficiency can be more readily achieved in parallel tandem cells without the strict criterion for photocurrent matching. CVD graphene satisfies most of the criteria for use as an IML for both parallel and series connections. CVD-grown graphene film (<1 kΩ/sq) with high transparency (>80% at 550 nm) has been demonstrated to be a good IML between two subcells, as shown in Figure 2b. The high in-plane conductivity of graphene prevents charge buildup between subcells. The work function of graphene is in the range between 4.2 and 4.6 eV, which is too low for efficient hole extraction. Efficient hole extraction can be achieved after coating graphene with MoO_3 to increase the work function to 5.5 eV.[48] By using graphene/MoO_3 IML in series-connected tandem cells, a favorable energy level offset was induced at the IML/subcells interfaces, leading to efficient recombination of electrons from the bottom cell and holes from the top cell. In parallel-connected tandem cells, the high work function of a sandwiched MoO_3/graphene/MoO_3 IML could extract the holes from ITO and LiF/Al cathodes effectively. As shown in Figure 2c,d, the values of open-circuit voltage (V_{oc}) and short-circuit current density (J_{sc}) in the tandem cell are very close to the sum values of V_{oc} and J_{sc} from the two single subcells in series and parallel connections, respectively, further confirming the good ohmic contact at the active layer/MoO_3-modified graphene interface. The nearly identical theoretical curve and experimental result obtained with the tandem cell (Figure 2d) suggests that a MoO_3/graphene/MoO_3 layer serves as an effective IML in parallel-connected tandem cells. Even without perfect current matching between two subcells, the efficiency of the parallel tandem cell can reach 88% of the sum of those of the two subcells.[48]

Solution-processed GO has also been applied as IML in series-connected tandem devices, as shown in Table 2.[49−51] Advantages include the ease of spin-coating GO, as well as its ability to form composites with polymer. Tung et al. mixed GO with conducting polymer PEDOT:PSS to make a sticky gel with higher electrical conductivity.[49] Using GO/PEDOT:PSS as an adhesive IML, two P3HT:PCBM bulk heterojunctions were stacked together by a direct adhesive lamination process without significant ohmic loss. The high V_{oc} of the tandem device was 0.94 V, reaching 84% of the sum of those of the two subcells. GO has also been mixed

DOI: 10.1021/jacs.5b10917
J. Am. Chem. Soc. 2016, 138, 1095−1102

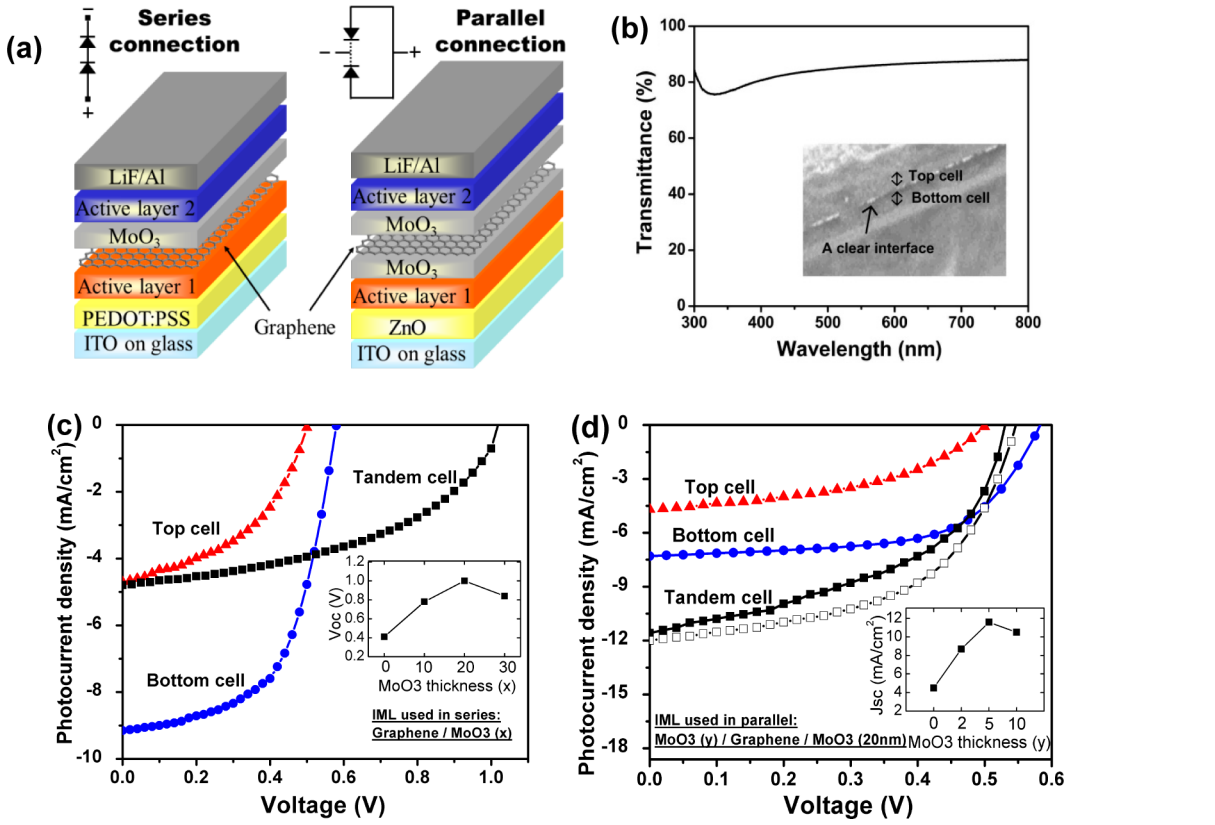

Figure 2. (a) Schematic diagram of photovoltaic device structure. (b) Transmittance spectrum of multi-layer graphene film. Inset: cross-sectional SEM image of the tandem device structure with graphene IML. Photocurrent characteristics ($J-V$ curve) of the top cell, bottom cell, and tandem cell devices with CVD-graphene intermediate layer under (c) series connection and (d) parallel connection. The theoretical $J-V$ curve of the tandem cell was constructed by summing the $J-V$ curves of the single cells (□). Inset graphs show the optimized thickness of MoO_3 in the tandem device. Reprinted with permission from ref 48. Copyright 2001 John Wiley and Sons.

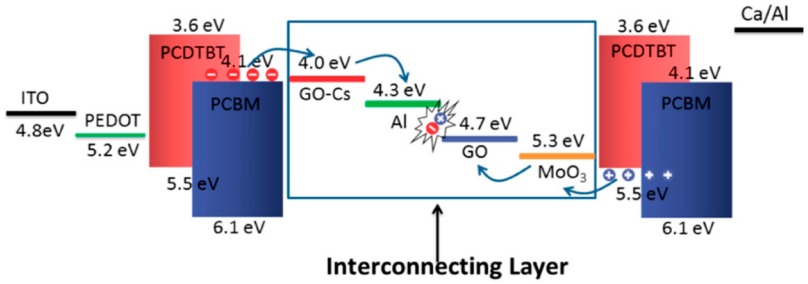

Figure 3. Schematic of the tandem device structure in which a GO-Cs/Al/GO/MoO_3 intermediate layer was employed. Reproduced with permission from ref 51. Copyright 2014 American Chemical Society.

with CNTs to form an IML for tandem OPVs using a similar approach.[50] Both standard and inverted tandem solar cells in series connection were fabricated with high V_{oc}, reaching 84% and 80% of the sum of those of the two subcells, respectively. Chen et al. reported a tandem OPV device with an IML consisting of GO-Cs/Al/GO/MoO_3, where GO-Cs refers to cesium-functionalized GO (Figure 3).[51] The work functions of GO-Cs and GO were both tuned in order to have perfect energy level matching between the subcells by surface engineering with Al and MoO_3, respectively. GO-based IMLs provide an efficient recombination region for electrons/holes generated from the subcells and yield a high V_{oc} = 1.69 V (~100% the sum of those of two subcells.)

With the recent material-based breakthroughs in solar cell research, PCE higher than 15% has already been achieved for various types of single devices. The next target for the solar research community would be to achieve a PCE higher than 20%, to match the performance of silicon-based photovoltaics. However, achieving such a high efficiency with a single device is challenging, owing to the trade-off between photocurrent gain and loss in V_{OC} for a small-bandgap photoactive layer. Thus, tandem cell architecture is considered to be a viable technology that can speed up the implementation of high-efficiency photovoltaics. Identifying the appropriate IML is necessary for enabling this technology in real applications. Graphene IMLs offer many advantages for tandem solar cells. One bottleneck in the use of CVD graphene is the lack of a non-handcrafted way for the high-throughput transfer of CVD graphene over a large area. Interface engineering of the graphene is also an important aspect to minimize energy loss with the adjacent subcells.

DOI: 10.1021/jacs.5b10917
J. Am. Chem. Soc. 2016, 138, 1095−1102

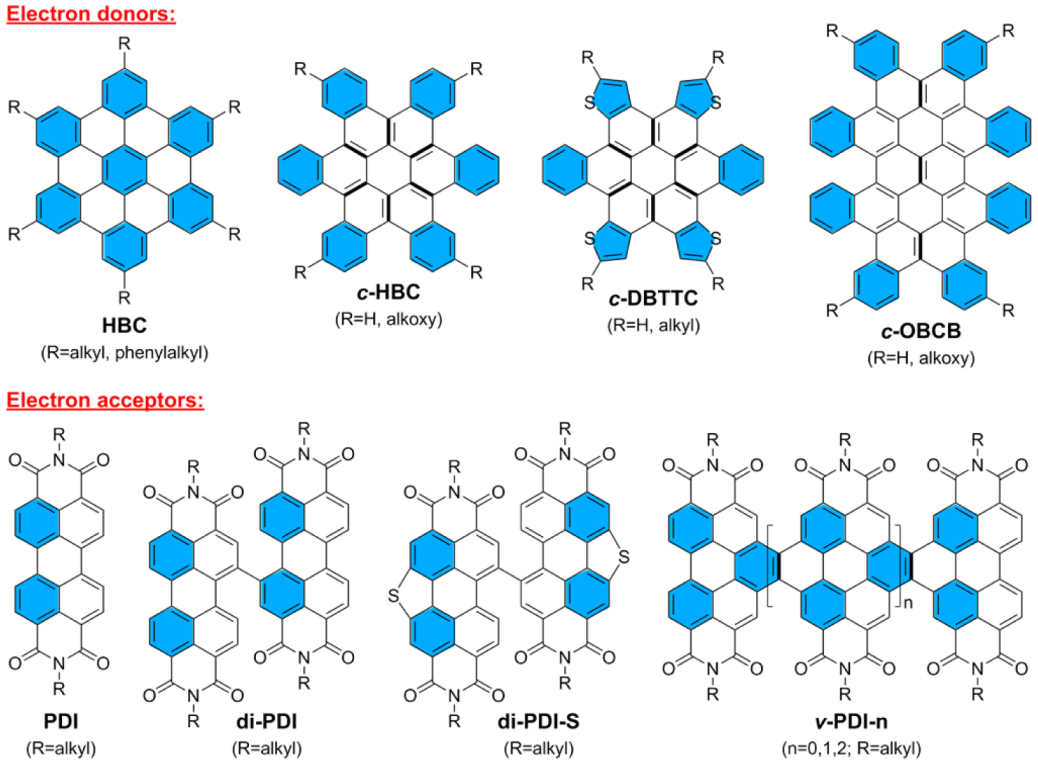

Figure 4. Structures of various graphene-like molecules used for organic solar cells.

GRAPHENE-LIKE MOLECULES FOR SOLAR CELLS

Benzenoid polycyclic aromatic hydrocarbons can be regarded as graphene-like molecules, and strong intermolecular $\pi-\pi$ interactions usually drive them into one-dimensional self-assembled columnar structures with high charge carrier mobility.[52] Depending on the electron-rich or electron-deficient nature, various graphene-like molecules have been used as either electron donors or electron acceptors in organic solar cells (Figure 4). Friend and Müllen first applied the disc-like liquid crystalline hexa-*peri*-hexabenzocoronene (**HBC**) together with a crystalline perylene diimide (**PDI**) in photodiodes and demonstrated efficient charge transfer between these two components.[53] This initialized the research into using solution-processible, small-molecule-based semiconductors for OPVs. However, the poor light-harvesting property of **HBC**, arising from its large number of aromatic sextet rings (the hexagons highlighted in blue in Figure 4), led to low PCEs. Later, Nuckolls's group synthesized a series of hexa-*cata*-hexabenzocoronenes (***c*-HBC**), which turned out to have a contorted, double-concave geometry.[54] ***c*-HBC** shows a radialene character for the central benzene ring and displays improved light-harvesting properties compared to its planar **HBC** counterparts. Interestingly, these non-planar molecules still can form long-range ordered columnar packing, with field-effect hole mobility up to 0.02 $cm^2/(V{\cdot}s)$ in the solution-processed thin films. In addition, the double-concave structure allows them to nest ball-shaped electron acceptors such as fullerene (C_{60}). In fact, bilayer heterojunction devices using parent ***c*-HBC** and C_{60} exhibited very efficient charge transfer at this optimal ball-and-socket interface, and high V_{oc} up to 0.95 V was achieved. However, the overall PCE was still low (1.04%) due to the still poor light-harvesting capability of the ***c*-HBC**.[55] This was further improved by using the thiophene analogues, the alkylated dibenzotetrathienocoronenes (***c*-DBTTC**), which show very intense absorption in the UV region and can form a self-assembled, three-dimensional network of cables.[56] This scaffold provided a template for a reticulated heterojunction with C_{60} and resulted in an improved PCE of ~2%. Ball-and-socket complexation was also found in the solution-processed thin films of ***c*-HBC**:$PC_{70}BM$[57] and ***c*-DBTTC**:$PC_{70}BM$,[58] leading to a maximum PCE of 2.41% for the latter. Bathochromic absorption was observed for the larger-sized contorted octabenzocircumbiphenyl (***c*-OBCB**); consequently, solar cells based on ***c*-OBCB**:$PC_{70}BM$ complexes gave PCEs up to 2.9%.[59] These studies showed that both light harvesting and molecular-scale donor–acceptor complexation play important roles in determining the solar cell's performance. Development should focus on how to improve light absorption in the visible and even the near-infrared regions, where absorption is weak.

Graphene-like molecules, when substituted by strong electron-withdrawing groups, can be converted into n-type semiconductors. One good example is **PDI**, which shows strong absorption in the visible region, high electron mobility, and a LUMO energy level comparable to that of typical fullerenes. Therefore, it was considered for use as a new non-fullerene acceptor in OPVs. Early tests using **PDI** as an electron acceptor in OPVs were not so successful, with a maximum PCE of ~4%, mainly due to the formation of too-large crystalline **PDI** domains. This situation was improved by using a twisted, bay-linked PDI dimer (**di-PDI**), which can form a homogeneous blend with a suitable donor polymer, giving a PCE of up to 6%.[60] Very recently, a PCE as high as 7.16% was achieved when a S-annulated PDI dimer (**di-PDI-S**) was used as acceptor.[61] On the other hand, Nuckolls et al. developed a series of vinyl-bridged PDI oligomers (***v*-PDI-*n***, n = 1–4) with a helical, ribbon-like structure.[62] These oligomers showed good solubility in normal organic solvents, intense absorption in the visible region, high electron mobility, and a low-lying LUMO energy level similar to

DOI: 10.1021/jacs.5b10917
J. Am. Chem. Soc. 2016, 138, 1095–1102

those of PCBMs. OPVs from the blend of these oligomers and appropriate donor polymers give a PCE as high as 8.3%, setting a record high for non-fullerene bulk heterojunctions. The good performance can be ascribed to the mesh-like network of acceptors with pores that are tens of nanometers in diameter for efficient exciton separation and charge transport. These research works demonstrate that electron-accepting graphene-like molecules with a twisted structure could be good replacements for expensive fullerene acceptors in OPVs. The key for further improvements relies on whether we can further enhance the light-harvesting capability, maintain high electron mobility, and find the right donor polymer to form an optimal morphology.

CONCLUSION

In summary, collective evidence from research over the years has shown that graphene, whether grown by CVD or solution-synthesized, has found niche roles in various components of solar cells, giving rise to performance enhancement. Instead of replacing silicon-based photovoltaics, it is more realistic to consider graphene as a performance enhancer in these devices. Bottom-up-synthesized graphene-like molecules have diverse structural motifs which can be tailor-made for various functions. Chemists are learning about the design principles in these molecules that can afford strong light harvesting and efficient exciton separation. In the future, it should be possible to realize a flexible solar cell consisting of a photoactive layer made from graphene-like molecules for absorption and exciton generation, and hole or electron transport layers made from solution-processed graphene, with all these components integrated on a flexible, large-area graphene electrode.

AUTHOR INFORMATION

Corresponding Author

*chmlohkp@nus.edu.sg

Notes

The authors declare no competing financial interest.

ACKNOWLEDGMENTS

The authors like to acknowledge funding support from MOE2014-T3-1-004.

REFERENCES

(1) Wang, Y.; Tong, S. W.; Xu, X. F.; Ozyilmaz, B.; Loh, K. P. *Adv. Mater.* **2011**, *23*, 1514−1518.
(2) Wang, Y.; Chen, X. H.; Zhong, Y. L.; Zhu, F. R.; Loh, K. P. *Appl. Phys. Lett.* **2009**, *95*, 063302.
(3) He, Z. C.; Zhong, C. M.; Su, S. J.; Xu, M.; Wu, H. B.; Cao, Y. *Nat. Photonics* **2012**, *6*, 591−595.
(4) Park, H.; Brown, P. R.; Bulovic, V.; Kong, J. *Nano Lett.* **2012**, *12*, 133−140.
(5) Wang, X.; Zhi, L.; Müllen, K. *Nano Lett.* **2008**, *8*, 323−327.
(6) Wang, X.; Zhi, L.; Tsao, N.; Tomović, Ž.; Li, J.; Müllen, K. *Angew. Chem., Int. Ed.* **2008**, *47*, 2990−2992.
(7) Park, H.; Chang, S.; Zhou, X.; Kong, J.; Palacios, T.; Gradečak, S. *Nano Lett.* **2014**, *14*, 5148−5154.
(8) Park, H.; Chang, S.; Zhou, X.; Kong, J.; Palacios, T.; Gradečak, S. *Nano Lett.* **2014**, *14*, 5148−5154.
(9) Yusoff, A. R. b. M.; Kim, D.; Schneider, F. K.; da Silva, W. J.; Jang, J. *Energy Environ. Sci.* **2015**, *8*, 1523−1537.
(10) Yusoff, A. R. b. M.; Lee, S. J.; Shneider, F. K.; da Silva, W. J.; Jang, J. *Adv. Energy Mater.* **2014**, *4*, 1301989.
(11) Stratakis, E.; Savva, K.; Konios, D.; Petridis, C.; Kymakis, E. *Nanoscale* **2014**, *6*, 6925−6931.
(12) Bonaccorso, F.; Sun, Z.; Hasan, T.; Ferrari, A. C. *Nat. Photonics* **2010**, *4*, 611−622.
(13) Liu, Y.; Yuan, L.; Yang, M.; Zheng, Y.; Li, L.; Gao, L.; Nerngchamnong, N.; Nai, C. T.; Sangeeth, C. S. S.; Feng, Y. P.; Nijhuis, C. A.; Loh, K. P. *Nat. Commun.* **2014**, *5*, 5461.
(14) Lee, S.; Yeo, J.-S.; Ji, Y.; Cho, C.; Kim, D.-Y.; Na, S.-I.; Lee, B. H.; Lee, T. *Nanotechnology* **2012**, *23*, 344013.
(15) Hsu, C.-L.; Lin, C.-T.; Huang, J.-H.; Chu, C.-W.; Wei, K.-H.; Li, L.-J. *ACS Nano* **2012**, *6*, 5031−5039.
(16) Park, H.; Rowehl, J. A.; Kim, K. K.; Bulovic, V.; Kong, J. *Nanotechnology* **2010**, *21*, 505204.
(17) Kim, K.; Bae, S.-H.; Toh, C. T.; Kim, H.; Cho, J. H.; Whang, D.; Lee, T.-W.; Özyilmaz, B.; Ahn, J.-H. *ACS Appl. Mater. Interfaces* **2014**, *6*, 3299−3304.
(18) Schedin, F.; Geim, A. K.; Morozov, S. V.; Hill, E. W.; Blake, P.; Katsnelson, M. I.; Novoselov, K. S. *Nat. Mater.* **2007**, *6*, 652−655.
(19) Ju, L.; Velasco, J., Jr.; Huang, E.; Kahn, S.; Nosiglia, C.; Tsai, H.-Z.; Yang, W.; Taniguchi, T.; Watanabe, K.; Zhang, Y.; Zhang, G.; Crommie, M.; Zettl, A.; Wang, F. *Nat. Nanotechnol.* **2014**, *9*, 348−352.
(20) Zhang, L.; Roy, S. S.; English, C. R.; Hamers, R. J.; Arnold, M. S.; Andrew, T. L. *ACS Nano* **2015**, *9*, 2510−2517.
(21) Wong, C. P. Y.; Koek, T. J. H.; Liu, Y. P.; Loh, K. P.; Goh, K. E. J.; Troadec, C.; Nijhuis, C. A. *ACS Appl. Mater. Interfaces* **2014**, *6*, 20464−20472.
(22) Chen, C. C.; Aykol, M.; Chang, C. C.; Levi, A. F. J.; Cronin, S. B. *Nano Lett.* **2011**, *11*, 1863−1867.
(23) Li, X. M.; Zhu, H. W.; Wang, K. L.; Cao, A. Y.; Wei, J. Q.; Li, C. Y.; Jia, Y.; Li, Z.; Li, X.; Wu, D. H. *Adv. Mater.* **2010**, *22*, 2743−2748.
(24) Song, Y.; Li, X.; Mackin, C.; Zhang, X.; Fang, W.; Palacios, T.; Zhu, H.; Kong, J. *Nano Lett.* **2015**, *15*, 2104−2110.
(25) Ho, P.-H.; Lee, W.-C.; Liou, Y.-T.; Chiu, Y.-P.; Shih, Y.-S.; Chen, C.-C.; Su, P.-Y.; Li, M.-K.; Chen, H.-L.; Liang, C.-T.; Chen, C.-W. *Energy Environ. Sci.* **2015**, *8*, 2085−2092.
(26) Dong, P.; Zhu, Y.; Zhang, J.; Hao, F.; Wu, J.; Lei, S.; Lin, H.; Hauge, R. H.; Tour, J. M.; Lou, J. *J. Mater. Chem. A* **2014**, *2*, 20902−20907.
(27) Hao, F.; Wang, Z.; Luo, Q.; Lou, J.; Li, J.; Wang, J.; Fan, S.; Jiang, K.; Lin, H. J. *J. Mater. Chem.* **2012**, *22*, 22756−22762.
(28) Jeon, I.; Chiba, T.; Delacou, C.; Guo, Y.; Kaskela, A.; Reynaud, O.; Kauppinen, E. I.; Maruyama, S.; Matsuo, Y. *Nano Lett.* **2015**, *15*, 6665−6671.
(29) Jeon, I.; Cui, K.; Chiba, T.; Anisimov, A.; Nasibulin, A. G.; Kauppinen, E. I.; Maruyama, S.; Matsuo, Y. *J. Am. Chem. Soc.* **2015**, *137*, 7982−7985.
(30) Dabera, G. D. M. R.; Prabhath, M. R. R.; Lai, K. T.; Jayawardena, K. D. G. I.; Sam, F. L. M.; Rozanski, L. J.; Adikaari, A. A. D. T.; Silva, S. R. P. *Adv. Funct. Mater.* **2015**, *25*, 4520−4530.
(31) Moon, I. K.; Kim, J. I.; Lee, H.; Hur, K.; Kim, W. C.; Lee, H. *Sci. Rep.* **2013**, *3*, 1112.
(32) Xu, Q.; Song, T.; Cui, W.; Liu, Y.; Xu, W.; Lee, S. T.; Sun, B. *ACS Appl. Mater. Interfaces* **2015**, *7*, 3272−3279.
(33) Yang, L.; Yu, X.; Hu, W.; Wu, X.; Zhao, Y.; Yang, D. *ACS Appl. Mater. Interfaces* **2015**, *7*, 4135−4141.
(34) Song, M.; You, D. S.; Lim, K.; Park, S.; Jung, S.; Kim, C. S.; Kim, D.-H.; Kim, D.-G.; Kim, J.-K.; Park, J.; Kang, Y.-C.; Heo, J.; Jin, S.-H.; Park, J. H.; Kang, J.-W. *Adv. Funct. Mater.* **2013**, *23*, 4177−4184.
(35) Kim, Y.; Ryu, T. I.; Ok, K.-H.; Kwak, M.-G.; Park, S.; Park, N.-G.; Han, C. J.; Kim, B. S.; Ko, M. J.; Son, H. J.; Kim, J.-W. *Adv. Funct. Mater.* **2015**, *25*, 4580−4589.
(36) Li, S.-S.; Tu, K.-H.; Lin, C.-C.; Chen, C.-W.; Chhowalla, M. *ACS Nano* **2010**, *4*, 3169.
(37) Wang, J. T.-W.; Ball, J. M.; Barea, E. M.; Abate, A.; Alexander-Webber, J. A.; Huang, J.; Saliba, M.; Mora-Sero, I.; Bisquert, J.; Snaith, H. J.; Nicholas, R. J. *Nano Lett.* **2014**, *14*, 724−730.
(38) Liu, T.; Kim, D.; Han, H.; Yusoff, A. R. M.; Jang, J. *Nanoscale* **2015**, *7*, 10708−10718.
(39) Yan, K.; Wei, Z.; Li, J.; Chen, H.; Yi, Y.; Zheng, X.; Long, X.; Wang, Z.; Wang, J.; Xu, J.; Yang, S. *Small* **2015**, *11*, 2269−2274.

DOI: 10.1021/jacs.5b10917
J. Am. Chem. Soc. 2016, 138, 1095−1102

(40) Yeo, J.-S.; Kang, R.; Lee, S.; Jeon, Y.-J.; Myoung, N.; Lee, C.-L.; Kim, D.-Y.; Yun, J.-M.; Seo, Y.-H.; Kim, S.-S.; Na, S.-I. *Nano Energy* **2015**, *12*, 96−104.
(41) Hadipour, A.; de Boer, B.; Wildeman, J.; Kooistra, F. B.; Hummelen, J. C.; Turbiez, M. G. R.; Wienk, M. M.; Janssen, R. A. J.; Blom, P. W. M. *Adv. Funct. Mater.* **2006**, *16*, 1897−1903.
(42) Sista, S.; Hong, Z.; Park, M.-H.; Xu, Z.; Yang, Y. *Adv. Mater.* **2010**, *22*, E77−E80.
(43) Guo, X. Y.; Liu, F. M.; Yue, W.; Xie, Z. Y.; Geng, Y. H.; Wang, L. X. *Org. Electron.* **2009**, *10*, 1174−1177.
(44) Shrotriya, V.; Wu, E. H.-E.; Li, G.; Yao, Y.; Yang, Y. *Appl. Phys. Lett.* **2006**, *88*, 064104.
(45) Guo, F.; Kubis, P.; Li, N.; Przybilla, T.; Matt, G.; Stubhan, T.; Ameri, T.; Butz, B.; Spiecker, E.; Forberich, K.; Brabec, C. J. *ACS Nano* **2014**, *8*, 12632−12640.
(46) Tanaka, S.; Mielczarek, K.; Ovalle-Robles, R.; Wang, B.; Hsu, D.; Zakhidov, A. A. *Appl. Phys. Lett.* **2009**, *94*, 113506.
(47) Xia, X.; Wang, S.; Jia, Y.; Bian, Z.; Wu, D.; Zhang, L.; Cao, A.; Huang, C. *J. Mater. Chem.* **2010**, *20*, 8478−8482.
(48) Tong, S. W.; Wang, Y.; Zheng, Y.; Ng, M.-F.; Loh, K. P. *Adv. Funct. Mater.* **2011**, *21*, 4430−4435.
(49) Tung, V. C.; Kim, J.; Cote, L. J.; Huang, J. *J. Am. Chem. Soc.* **2011**, *133*, 9262−9265.
(50) Tung, V. C.; Kim, J.; Huang, J. *Adv. Energy Mater.* **2012**, *2*, 299−303.
(51) Chen, Y.; Lin, W.-C.; Liu, J.; Dai, L. *Nano Lett.* **2014**, *14*, 1467−1471.
(52) Wu, J.; Pisula, W.; Müllen, K. *Chem. Rev.* **2007**, *107*, 718−747.
(53) Schmidt-Mende, L.; Fechtenkötter, A.; Müllen, K.; Moons, E.; Friend, R. H.; MacKenzie, J. D. *Science* **2001**, *293*, 1119−1122.
(54) Xiao, S.; Myers, M.; Miao, Q.; Sanaur, S.; Pang, K.; Steigerwald, M. L.; Nuckolls, C. *Angew. Chem., Int. Ed.* **2005**, *44*, 7390−7394.
(55) Tremblay, N. J.; Gorodetsky, A. A.; Cox, M. P.; Schiros, T.; Kim, B.; Steiner, R.; Bullard, Z.; Sattler, A.; So, W.-Y.; Itoh, Y.; Toney, M. F.; Ogasawara, H.; Ramirez, A. P.; Kymissis, I.; Steigerwald, M. L.; Nuckolls, C. *ChemPhysChem* **2010**, *11*, 799−803.
(56) Gorodetsky, A. A.; Chiu, C. Y.; Schiros, T.; Palma, M.; Cox, M.; Jia, Z.; Sattler, W.; Kymissis, I.; Steigerwald, M.; Nuckolls, C. *Angew. Chem., Int. Ed.* **2010**, *49*, 7909−7912.
(57) Kang, S. J.; Ahn, S.; Kim, J. B.; Schenck, C.; Hiszpanski, A. M.; Oh, S.; Schiros, T.; Loo, Y. L.; Nuckolls, C. *J. Am. Chem. Soc.* **2013**, *135*, 2207−2212.
(58) Kang, S. J.; Kim, J. B.; Chiu, C. Y.; Ahn, S.; Schiros, T.; Lee, S. S.; Yager, K. G.; Toney, M. F.; Loo, Y. L.; Nuckolls, C. *Angew. Chem., Int. Ed.* **2012**, *51*, 8594−8597.
(59) Xiao, S.; Kang, S. J.; Wu, Y.; Ahn, S.; Kim, J. B.; Loo, Y. L.; Siegrist, T.; Steigerwald, M. L.; Li, H. X.; Nuckolls, C. *Chem. Sci.* **2013**, *4*, 2018−2023.
(60) Zang, Y.; Li, C. Z.; Chueh, C. C.; Williams, S. T.; Jiang, W.; Wang, Z. H.; Yu, J. S.; Jen, A. K. Y. *Adv. Mater.* **2014**, *26*, 5708−5714.
(61) Sun, D.; Meng, D.; Cai, Y.; Fan, B.; Li, Y.; Jiang, W.; Huo, L.; Sun, Y.; Wang, Z. *J. Am. Chem. Soc.* **2015**, *137*, 11156−11162.
(62) Zhong, Y.; Trinh, M. T.; Chen, R.; Purdum, G. E.; Khlyabich, P. P.; Sezen, M.; Oh, S.; Zhu, H.; Fowler, B.; Zhang, B.; Wang, W.; Nam, C.-Y.; Sfeir, M. Y.; Black, C. T.; Steigerwald, M. L.; Loo, Y.-L.; Ng, F.; Zhu, X.-Y.; Nuckolls, C. *Nat. Commun.* **2015**, *6*, 8242.

DOI: 10.1021/jacs.5b10917
J. Am. Chem. Soc. 2016, 138, 1095−1102